Biomass Conversion and Biorefinery (2023) 13:16441–16451
https://doi.org/10.1007/s13399-023-04000-7

ORIGINAL ARTICLE

Thermogravimetric and kinetic studies on pyrolysis of empty fruit bunch over metal-impregnated rice husk ash catalysts

Nadhilah Aqilah Shahdan[1] · Vekes Balasundram[1] · Norazana Ibrahim[2] · Ruzinah Isha[3]

Received: 2 November 2022 / Revised: 22 February 2023 / Accepted: 23 February 2023 / Published online: 2 March 2023

Abstract

Empty fruit bunch (EFB) is a biomass residue from palm oil plantations, abundant in tropical countries like Malaysia. EFB is a valuable resource when utilized for energy recovery. Rice husk ash (RHA), retrieved after pyrolyzing and calcining rice husks, has high silica content and is a low-cost alternative to conventional silica precursors. This study utilizes RHA as a silica precursor for catalyst synthesis, labelled CRHA. CRHA is metal-modified using nickel and iron, forming NiCRHA, FeCRHA and NiFeCRHA catalysts. The synthesized catalysts were applied to the pyrolysis of EFB and compared with HZSM-5 via thermogravimetric analyser (TGA). From TGA, CRHA produced similar amount of volatilized matter (75.1 wt%) to HZSM-5 catalyst (73.3 wt%) while using NiCRHA resulted in the highest amount of volatilized matter (83.9 wt%) among the catalytic runs. Kinetic analysis from the application of Coats-Redfern method showed that the non-catalytic run followed a one-dimensional diffusion while the catalytic runs followed the anti-Jander diffusion. The activation energy, E_a, was overall reduced from 74.15 kJ·mol^{-1} with the presence of the catalysts in the order of: 69.64 kJ·mol^{-1} (EFB-NiCRHA) > 64.28 kJ·mol^{-1} (EFB-CRHA) > 63.57 kJ·mol^{-1} (EFB-NiFeCRHA) > 58.77 kJ·mol^{-1} (EFB-FeCRHA) > 53.81 kJ·mol^{-1} (EFB-HZSM-5). Despite NiCRHA having the highest E_a among the catalytic runs, it also had the highest pre-exponential factor (1.48×10^4 min^{-1}) allowing the reaction to overcome the energy barrier and volatilized the most matter. This study showed that low-cost alternative sources can be used for catalysts synthesis and applied to thermochemical processes like pyrolysis.

Keywords Pyrolysis · Empty fruit bunch · Rice husk ash · Metal-modification · Thermogravimetric analysis · Kinetic analysis

1 Introduction

Biomass is an attractive source of material because it is renewable and relatively abundant. It is currently being studied as an alternative source to non-renewable materials like fossil fuels. Agricultural residues, a type of biomass, are often discarded as it is a by-product of agricultural crops. Such agricultural residues include wheat straw, sugarcane bagasse and empty fruit bunch (EFB) [1–3]. However, these low-cost materials should be retrieved as they may contain valuable chemicals, such as hydrocarbons. In tropical countries like Malaysia, palm oil industry is one of the main agricultural industries, and from the palm oil processing, a large percentage of about 70% is recovered in the form by-products, which includes EFB [4]. From available data in 2017, 7.7 Mt of EFB available in Malaysia was reported to have energy potential of 146.9 PJ [5]. EFB can be disposed of via incineration. However, due to its contribution to air pollution, the practice has been prohibited by the Malaysian government and thus, most EFB remain unutilized [6]. Therefore, the utilization of EFB in energy recovery is encouraged to divert this resource from landfills and retrieve its valuable chemicals.

Chemicals can be retrieved from biomass in the form of bio-oil through thermochemical processes such as pyrolysis, which thermally degrades materials in an air-free environment at temperatures between 300 °C and 700 °C [7]. For

✉ Vekes Balasundram
vekes@utm.my

[1] Malaysia-Japan International Institute of Technology, Universiti Teknologi Malaysia, 54100 Kuala Lumpur, Malaysia

[2] Energy Research Group, School of Chemical and Energy Engineering, Faculty of Engineering, Universiti Teknologi Malaysia, 81310 Johor Bahru, Johor, Malaysia

[3] College of Engineering, Universiti Malaysia Pahang, 26600 Pekan, Pahang, Malaysia

EFB-derived bio-oil specifically, previous studies mentioned the advantageous feature of lower sulphur content of the bio-oil when compared to petroleum fuel [8]. However, biomass-derived bio-oil is unstable and high in oxygen content, due to compounds like alcohols, acids, and ketones, that are present which limits the use of the bio-oil commercially [9]. Thus, research and development is on-going to improve the properties of the bio-oil.

The addition of catalysts to a pyrolysis process is one of the methods to improve bio-oil properties. Catalysts help to reduce oxygen content in the bio-oil by promoting secondary reactions and deoxygenation reactions via its catalyst pores [7]. A review conducted by Kan et al. (2020) that discussed the variation of process parameters of catalytic pyrolysis of biomass introduced that the HZSM-5 catalyst is an attractive catalyst for this process as it encourages the formation of hydrocarbons and reduces the number of oxygenated compounds due to the microporous structure and suitable acidity of the catalyst [10].

Moreover, modification of the catalysts can be done by impregnating metal species onto the catalyst. For instance, the two types of metals that are inexpensive and widely available, nickel and iron, can promote aromatization and can prevent polymerization of important compounds like monocyclic aromatic hydrocarbons (MAHs) [11, 12]. These two metals can be modified by the wet impregnation method which is a simple procedure that has shown to be successfully applied to the catalyst in previous studies [13, 14]. HZSM-5 catalysts can be synthesized using a silica source, alumina source, an organic template, and an alkali compound [15]. Due to the harmful chemicals, such as tetraethylorthosilicate (TEOS), used for catalyst synthesis and a rising interest in renewable materials, rice husk ash (RHA), another renewable resource, has been used as an alternative silica source for catalyst synthesis due to its high silica content of around 93% [16]. Previous studies have shown the successful synthesis of HZSM-5 catalysts using RHA as a silica source but not the application of the synthesized catalyst especially in pyrolysis [17, 18]. There are also lack of studies on whether or not the synthesized catalysts can be metal-modified.

Thermogravimetric analyser (TGA) can be used to observe the degradation of feedstock for a small sample size often between 5 to 50 mg [19]. Inert atmosphere can be created with the inert gas of choice to achieve the pyrolysis condition. The mass loss and the rate of mass loss can be observed with TGA to investigate how the feedstock can be affected, for example, with the presence of catalyst. The data collected from TGA can then be used to conduct kinetic analysis, where kinetic parameters such as activation energy and the pre-exponential factor can be mathematically determined, using method-fitting methods such as Coats-Redfern (CR) method [20]. The Coats-Redfern method gives an insight to the possible mechanism that occurs during the reaction while only requiring one heating rate [21].

This current work studies the pyrolysis of EFB over catalysts synthesized using RHA as the silica source and catalysts that are metal-modified with nickel and iron via thermogravimetric analyser. In addition, kinetic analysis via Coats-Redfern method was conducted to further analyse the impact of the catalyst presence on the pyrolysis of EFB.

2 Materials and methods

2.1 Raw material preparation

Empty fruit bunch (EFB), a type of waste generated from palm oil production, was used as the biomass feedstock, purchased from Selangor, Malaysia. EFB was dried to remove any remaining moisture and grounded into uniform particle sizes of 0.5 mm. Rice husks were purchased from another local company in Selangor, Malaysia. The rice husks were washed with deionized (DI) water, dried in a laboratory oven, and grounded into smaller particle sizes of 0.5 mm. The rice husks were then pyrolyzed in a tube furnace at a temperature of 750 °C for 1 h in a nitrogen atmosphere to obtain black rice husk ash (RHA). Next, the black RHA was calcined in a muffle furnace at 750 °C for 3 h to obtain white RHA. White RHA was used as the silica precursor for catalyst synthesis.

2.2 Catalyst preparation and characterization

The prepared white RHA was used to synthesize the catalyst by mixing it with sodium aluminate, tetrapropylammonium bromide (TPABr) and sodium carbonate decahydrate in a beaker with a molar composition of 30 SiO_2: Al_2O_3:3.75 TPABr:9 $Na_2CO_3 \cdot 10H_2O$, obtained from a study from Zhang et al. (2019) [18]. The mixture was mixed for 10 min using a mortar and pestle before being transferred into a Teflon-lined autoclave reactor and placed in a laboratory oven for heating at 145 °C for 72 h. After the sample was taken out of the oven, the sample was washed with DI water, filtered, and further dried in the same oven at 110 °C overnight. Finally, the sample was calcined in a muffle furnace at 750 °C for 4 h and labelled as 'CRHA', indicating that the catalyst was made using RHA. Table 1 shows the elemental characterization of the white RHA and the synthesized CRHA. Note that CRHA contained Br due to the presence of TPABr during synthesis. Trace compounds in Table 1 consisted of the sum of compounds that contained less than 0.01% each, which were TiO_2, Cr_2O_3, NiO, CuO, ZnO, Rb_2O and SrO.

For the metal-modification of the catalysts, metals Ni and Fe were impregnated using the wet impregnation

Table 1 Elemental characterization of white RHA and CRHA

Compound	Composition (%)	
	White RHA	CRHA
SiO_2	94.681	91.739
Al_2O_3	1.039	1.734
MgO	1.449	4.214
K_2O	1.139	0.304
P_2O_5	0.661	0.726
CaO	0.601	0.287
Cl	0.212	0.240
Fe_2O_3	0.075	0.085
MnO	0.070	0.081
SO_3	0.037	0.136
Eu_2O_3	0.012	4.214
Br	0.000	0.439
Trace compounds	0.022	0.016

method. Nickel (II) nitrate hexahydrate, $Ni(NO_3)_2{\cdot}6H_2O$ (purity = 97%) was added at a 5 wt% to CRHA and mixed with 80 mL of DI water in a beaker. The mixture was stirred for 4 h at 80 °C on a magnetic stir plate. The mixture was then filtered and dried overnight in an oven at 110 °C. Calcination was then conducted on the catalyst sample at 750 °C for 4 h. This catalyst was labelled as 'NiCRHA'. The metal-modified catalyst, 'FeCRHA', was impregnated with 5 wt% Fe using iron (III) nitrate nonahydrate, $Fe(NO_3)_3{\cdot}9H_2O$ (purity = 99%) following the same procedure. Another metal-modified catalyst, 'NiFeCRHA', was impregnated with 2.5 wt% Ni and 2.5 wt% Fe using the same chemicals and procedure as the previous two catalysts.

HZSM-5 was prepared as a benchmark for the previous three synthesized catalysts. From the ZSM-5 in ammonium form obtained from Alfa Aesar, calcination was conducted in a muffle furnace at 750 °C for 4 h to obtain HZSM-5.

The synthesized catalysts were characterized to analyze their physicochemical properties. Characterization methods that were conducted include phase analysis using X-ray Diffraction (XRD), surface morphology analysis using Field Emission Scanning Electron Microscopy (FESEM), surface area and pore size analysis using Brunauer–Emmett–Teller (BET) method and the framework vibrational analysis using Fourier Transform Infrared spectroscopy (FTIR). Details on the characterization methods can be referred to in our previous work [22].

2.3 Experimental setup

The first set of experiment was conducted using thermogravimetric analyser (TA Instrument, DE, USA). Nitrogen was used as the inert gas for pyrolysis, with a flow rate of 100 mL/min. Approximately 4 mg of sample was loaded on an aluminum crucible into the thermogravimetric analyser. For the catalytic runs, a catalyst-to-feedstock ratio of 1:1 was used as a standard for this study, as a ratio of 1:1 was sufficient to produce results in comparison to non-catalytic runs seen from previous literature [23, 24]. In total, six runs were conducted, labelled as EFB, EFB-HZSM-5, EFB-CRHA, EFB-NiCRHA, EFB-FeCRHA and EFB-NiFeCRHA. Samples were heated up from 30 °C to 700 °C at a heating rate of 20 °C/min. The thermogravimetric (TG) and derivative thermogravimetric (DTG) curves were collected for thermogravimetric and kinetic analysis.

The kinetics of the pyrolysis processes were analysed using the Coats-Redfern (CR) integral method to determine the activation energy, E_a, and the pre-exponential factor, A. The derivation of the CR method, which can be referred to in our previous work [25], leads to the linearized expression of the CR method, shown below,

$$\ln\left[\frac{g_n(\alpha)}{T^2}\right] = \ln\left[\frac{AR}{\beta E_a}\left(1-\frac{2RT}{E_a}\right)\right] - \frac{E_a}{RT} \quad (1)$$

where α is the fractional conversion of the sample, $g_n(\alpha)$ is a reaction model in terms of α, n is the model number, T is the temperature in Kelvin, R is the gas constant (0.0083144 $kJ{\cdot}mol^{-1}{\cdot}K^{-1}$) and β is the heating rate (K/min). Table 2 shows the various kinetic models applied in this study [21]. The kinetic parameters, E_a and A, can be calculated by plotting the values obtained from applying the models in Table 2 into Eq. 1 into an *xy*-plot and determining the values from the slope and y-intercept of the plot.

3 Results and discussion

3.1 Catalyst characterization

3.1.1 Phase analysis

Figure 1 shows the XRD for the five synthesized catalysts. Overall, all the catalysts show narrow peaks indicating the high crystallinity of the catalysts. Figure 1(a) shows the XRD pattern of commercial HZSM-5, which was used as a benchmark for the other synthesized catalysts. The peaks seen at the 2θ position ranges of between 8.0° and 9.0°, between 13.0° and 17° and between 21° and 23°, are considered the characteristic peaks of HZSM-5 [18]. In Fig. 1(b), similar peaks in the same 2θ position ranges were observed for CRHA, indicating that HZSM-5 structure was able to be synthesized using RHA as the silica precursor. For NiCRHA, FeCRHA and NiFeCRHA catalysts, shown in Fig. 1(c), 1(d) and 1(e) respectively, it was expected that peaks representing NiO and Fe_3O_4 species were to be observed within the 37° and 43° range but this

Table 2 Various reaction models for solid state-reactions

Reaction Model	g(α)	Model Label
Chemical Reaction Model		
Zero order reaction ($n=0$)	α	R0
First order reaction ($n=1$)	$-\ln(1-\alpha)$	R1
Second order reaction ($n=2$)	$(1-\alpha)^{-1}-1$	R2
Third order reaction ($n=3$)	$([(1-\alpha)^{-2}-1]/2)$	R3
Diffusion Model		
1D diffusion	α^2	D1
2D diffusion (Valensi)	$\alpha+(1-\alpha)\ln(1-\alpha)$	D2
3D diffusion (Jander)	$[1-(1-\alpha)^{1/3}]^2$	D3
3D diffusion (Ginstling-Broushtein)	$(1—2\alpha/3)-(1-\alpha)^{2/3}$	D4
3D diffusion (anti-Jander)	$[(1+\alpha)^{1/3}-1]^2$	D5
3D diffusion (Zhrualev, Lesokin, Tempelmen)	$([1/(1-\alpha)]^{1/3}-1)^2$	D6
Nucleation and Nuclei Growth Model		
Power Law ($n=2$)	$\alpha^{1/2}$	PL2
Power Law ($n=3$)	$\alpha^{1/3}$	PL3
Geometric Contracting Model		
Contracting cylinder	$1-(1-\alpha)^{1/2}$	C1
Contracting cube or sphere	$1-(1-\alpha)^{1/3}$	C2

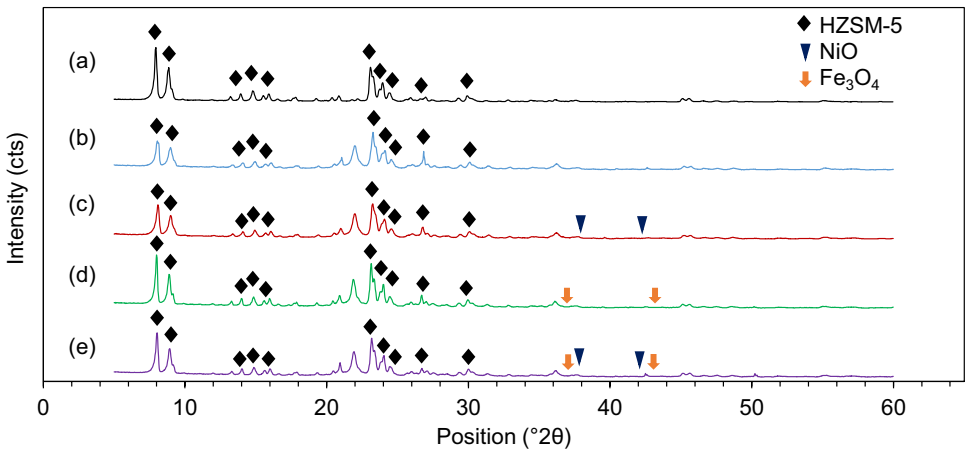

Fig. 1 XRD pattern for (**a**). HZSM-5, (**b**). CRHA, (**c**). NiCRHA, (**d**). FeCRHA and (**e**). NiFeCRHA

was not observed. According to a previous study by Cheng et al. (2017), the peaks representing the metal species was visible with a high metal loading of 10 wt% onto the catalyst [26]. However, in this study, a lower metal loading of 5 wt% was used and this could contribute to the absence of the peaks related to metal species. This instance also occurred in one of our previous studies, where loading 6 wt% of a different type of metal onto a HZSM-5 catalyst resulted in the absence of the peak representing the metal in the XRD pattern [27]. Furthermore, it can be implied, for the metal-modified catalysts, that the metal species were highly dispersed as no amorphous phase were observed and that the metal impregnation did not modify the original structure of the synthesized catalysts as the original XRD pattern was retained.

3.1.2 Framework vibrational analysis

Figure 2 shows the FTIR spectra for the synthesized catalysts. The characteristic vibration bands for HZSM-5 includes the ones around the wavenumbers 540 cm^{-1} and 1220 cm^{-1}, indicating the double 5-ring structure of HZSM-5, and around the wavenumbers 795 cm^{-1} and 1060 cm^{-1}, indicating the presence of $Si(Al)O_4$ asymmetric stretching, which can be seen in Fig. 2(a) [18]. For the synthesized catalyst CRHA, in Fig. 2(b), this presence of these vibration bands can be observed, which further confirmed that the HZSM-5 structure was achieved. With metal-modification of the CRHA, as seen in Fig. 2(c), 2(d) and 2(e), the parent catalyst structure of the RHA catalyst was not affected by the presence of metal species NiO and Fe_3O_4 as

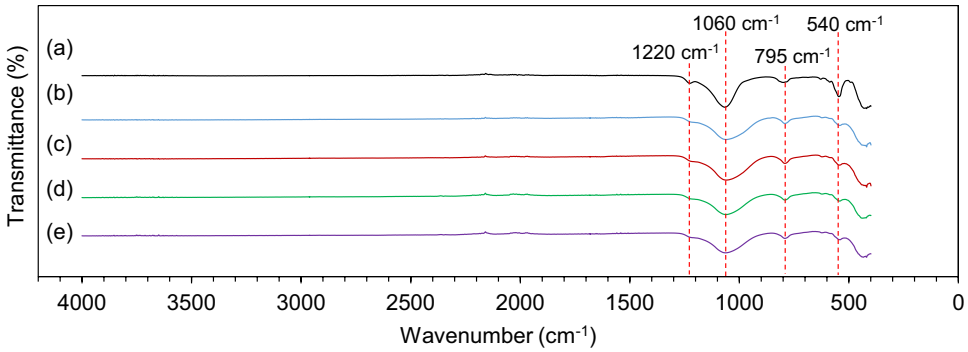

Fig. 2 FTIR spectra for (**a**). HZSM-5, (**b**). CRHA, (**c**). NiCRHA, (**d**). FeCRHA and (**e**). NiFeCRHA

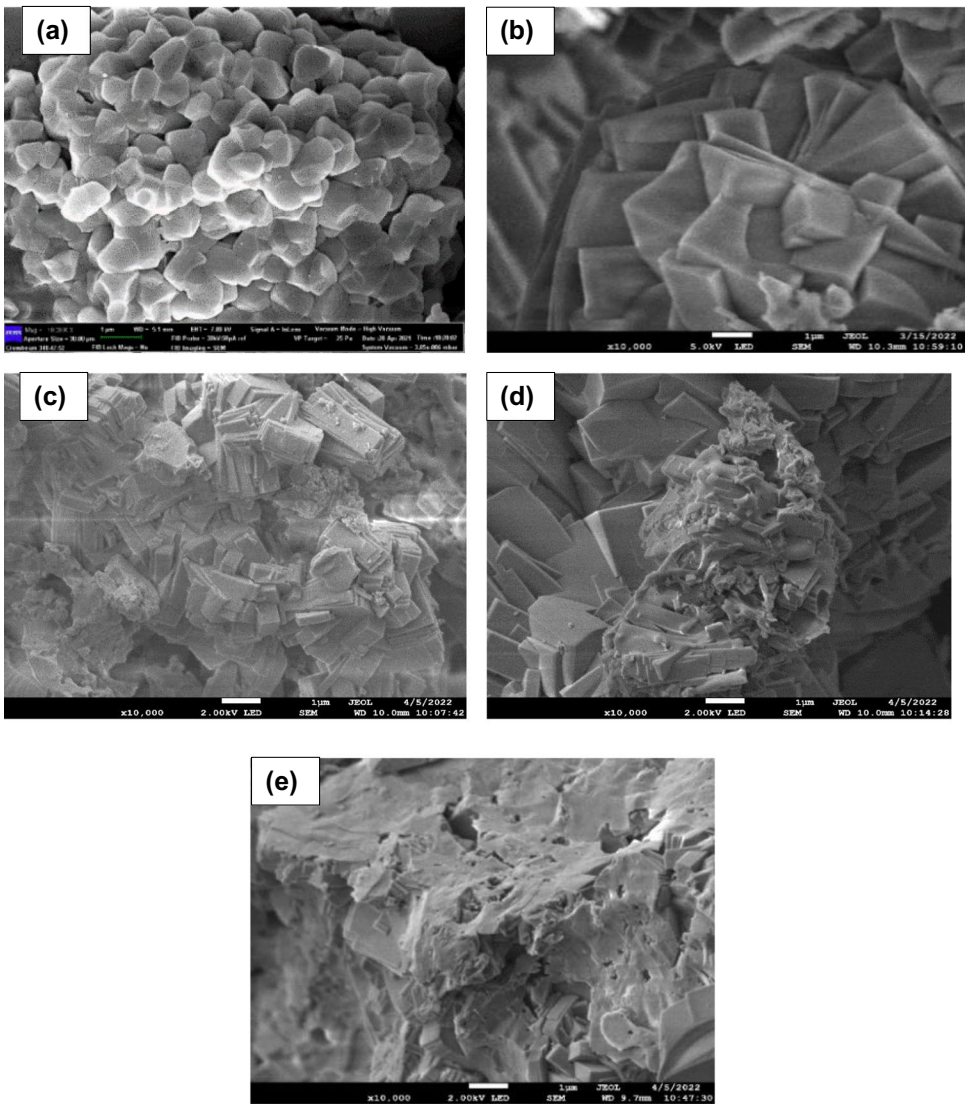

Fig. 3 FESEM images for (**a**). HZSM-5, (**b**). CRHA, (**c**). NiCRHA, (**d**). FeCRHA and (**e**). NiFeCRHA

the absorption bands around the wavenumbers 540 cm^{-1}, 795 cm^{-1}, 1060 cm^{-1} and 1220 cm^{-1} were visible.

3.1.3 Surface morphology analysis

The surface morphology of the synthesized catalysts is shown in Fig. 3(a – e). Figure 3(a) shows that the surface morphology of HZSM-5 catalyst has cubic-like particles that are irregular. The synthesized CRHA in Fig. 3(b) showed a much more crystalline structure compared to HZSM-5 with edges more defined. This high crystalline structure seen was in agreement to the narrow XRD peaks in Fig. 1(b). Zhang et al. (2019) used the same catalyst synthesis method and obtained similar crystalline particles [18]. With the addition of metals onto the catalyst, both NiCRHA and FeCRHA, in Fig. 3(c) and 3(d) respectively, appeared to have deposits formed on the catalyst surface, due to the deposition of metal species, NiO and Fe_3O_4. This occurrence also was observed by Chen et al. (2016), with the deposition of Ni onto HZSM-5 forming coarse surfaces on the parent catalyst [28]. For NiFeCRHA in Fig. 3(e), a layering covering the parent catalyst was observed with the addition of both NiO and Fe_3O_4 species.

3.1.4 Surface area and porosity analysis

Table 3 shows the surface area and pore properties of HZSM-5, CRHA, NiCRHA, FeCRHA and NiFeCRHA catalysts. The synthesized catalysts were compared with the results obtained from conventional HZSM-5. CRHA had a smaller BET surface area (205.16 m^2/g) compared to HZSM-5 (365.81 m^2/g). This agreed with the information obtained from the FESEM images where the particles of CRHA in Fig. 3(b) were observed to be larger in size compared to the particles of HZSM-5 in Fig. 3(a). Furthermore, the total pore volume and pore diameter of CRHA were both larger than that of HZSM-5 as seen in Table 1. With the impregnation of metal species onto the CRHA, the BET surface area reduced to 166.71 m^2/g, 181.33 m^2/g, and 184.02 m^2/g for NiCRHA, FeCRHA and NiFeCRHA respectively. Similarly, the total pore volume and pore diameter also reduced and the values are shown in Table 1. Nishu et al. (2022) also observed a similar occurrence where the deposition of metals on to the parent catalyst lead to the overall reduction in the BET surface area and total pore volume [29]. This is due to the deposition and accumulation of metal species inside the pores and the catalyst surfaces.

Table 3 Textural properties of the synthesized catalysts

Catalyst	BET Surface Area[a] (m^2/g)	Total Pore Volume[b] (cm^3/g)	Average Pore Diameter[c] (nm)
HZSM-5	365.81	0.0483	3.87
CRHA	205.16	0.1206	4.06
NiCRHA	166.71	0.1007	3.73
FeCRHA	181.33	0.1066	3.48
NiFeCRHA	184.02	0.1090	3.54

[a] the BET surface area was obtained by the BET method [30]

[b] the total pore volume was determined from the absorbed amount of $P/P_0 = 0.99$ [14]

[c] the average pore diameter was obtained from the adsorption branches of the isotherms by the BJH method [31]

3.2 Catalytic pyrolysis of EFB

3.2.1 Thermogravimetric analysis

The degradation patterns in the form of TG curves, the phase breakdown of the volatilized matter and the DTG curves for the non-catalytic and catalytic EFB pyrolysis is shown in Fig. 4, 5, and 6. The non-catalytic EFB run was conducted twice and the error was found to be within 0.1 wt% (not visible in Fig. 4 and 5). Catalyst mass was first removed by subtraction before further calculations in order to better

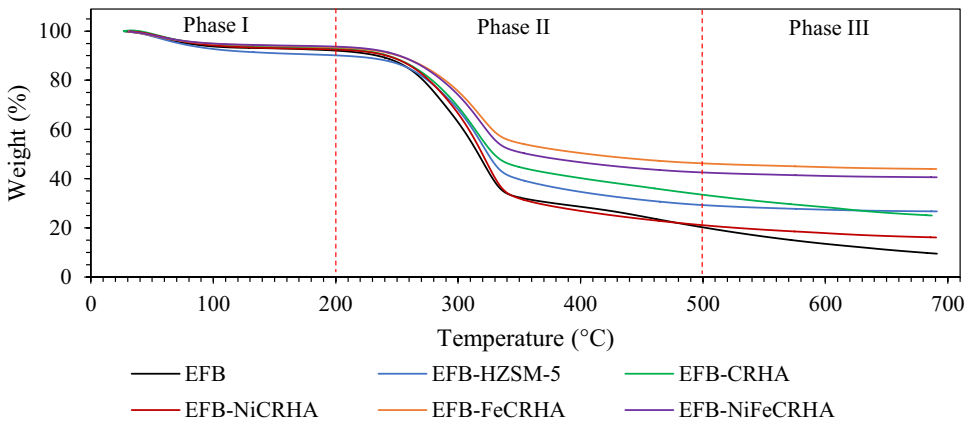

Fig. 4 TG curves for non-catalytic and catalytic EFB pyrolysis runs over HZSM-5 and synthesized catalysts (catalyst-to-feedstock = 1:1, heating rate = 20 °C/min)

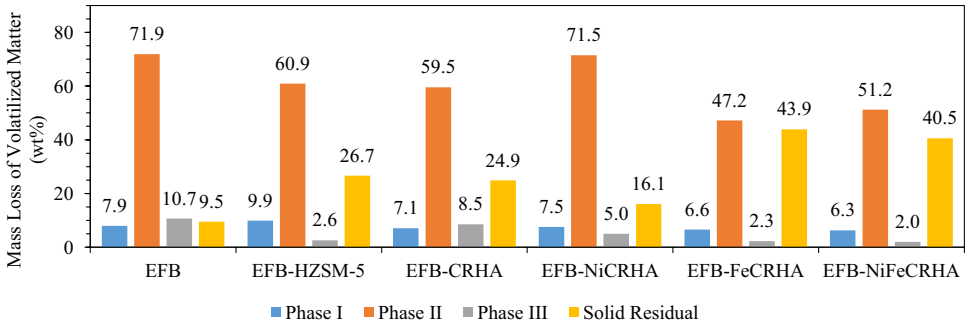

Fig. 5 Phase breakdown of volatilized matter for non-catalytic and catalytic EFB pyrolysis runs over HZSM-5 and synthesized catalysts (catalyst-to-feedstock = 1:1, heating rate = 20 °C/min)

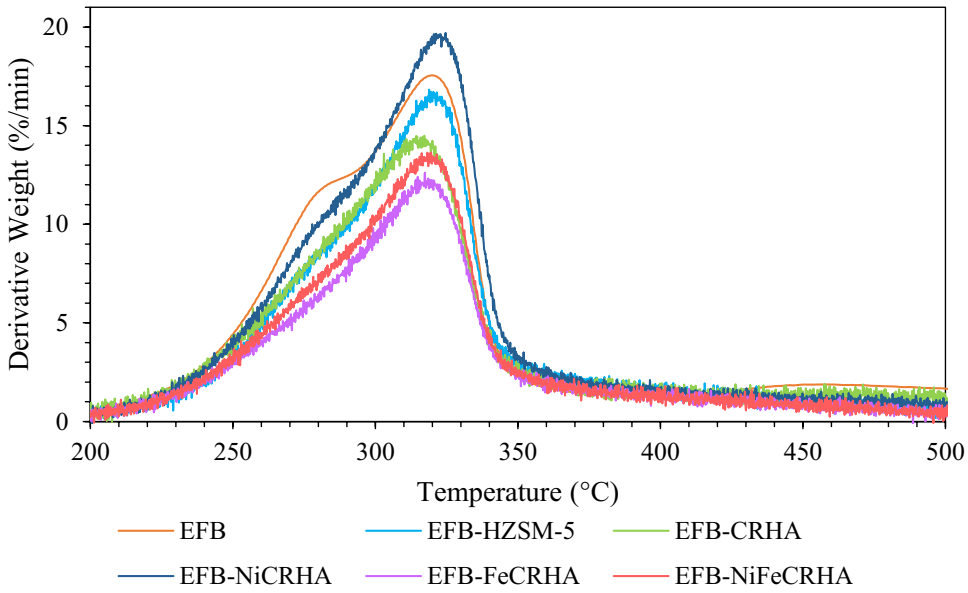

Fig. 6 DTG curves for non-catalytic and catalytic EFB pyrolysis runs over HZSM-5 and synthesized catalysts focused on Phase II (catalyst-to-feedstock = 1:1, heating rate = 20 °C/min)

observe the feedstock degradation. The degradation of EFB was divided into three phases, namely the vaporization of moisture (Phase I), the rapid degradation of lignocellulosic materials of EFB (Phase II) and the slowing down of degradation (Phase III). The general pattern of degradation of EFB that was observed in this study agreed with previous literature, where degradation was rapid in Phase II [32]. As mentioned by Wang et al. (2021), lignocellulose mainly consists of hemicellulose, cellulose and lignin, which degrades between temperature ranges 220 °C to 315 °C, 315 °C to 400 °C and 160 °C to 900 °C respectively [32].

For the catalytic runs, it was seen that overall, the TG curves shift upwards within the second and third phases, resulting in the increase of solid residual, as seen in Fig. 4. The synthesized catalyst, CRHA, performed similarly to HZSM-5 in degrading EFB, where both cases resulted in relatively similar amount of solid residual, 24.9 wt% and 26.7 wt%, respectively, as seen in Fig. 5. Moreover, the performance of the metal-modified catalysts in degrading the feedstock can also be observed from the amount of solid residual left for each run. The highest amount of solid residual left was obtained when FeCRHA was used (43.9 wt%) followed by when NiFeCRHA was used (40.5 wt%). The presence of NiCRHA, however, led to the least amount of solid residual (16.1 wt%) among the different catalysts used. According to a study conducted by Persson et al. (2019), Ni has a better cracking performance than Fe when impregnated onto HZSM-5 catalyst that would produce higher gas yield, which would explain the lower bio-oil and higher gas yield achieved when NiCRHA was used compared to FeCRHA [11]. Overall, it can be seen that the amount of solid residual when using the synthesized catalysts ranged from as low as 16.1 wt% to as high as 43.9 wt% for the catalytic runs of pyrolysis of EFB. Furthermore, the DTG pattern for the non-catalytic EFB run focused on Phase II in Fig. 6 showed a peak in Phase II with two humps, implying that the degradation of the individual lignocellulose components could overlap with each other within the same temperature range. The temperature at the maximum peak for EFB lies at 320 °C, close to the value reported by a previous study [33], while for the catalytic runs, temperature at the maximum peak ranged between 317 °C and 324 °C. This overlapping

of the curves also was observed with catalytic runs, although the distinction of multiple peaks was more obscured.

3.2.2 Kinetic analysis

Data obtained from the thermogravimetric analyser in Sect. 3.2.1 was applied to the Coats-Redfern (CR) method for kinetic analysis within the temperature range of 200 °C and 360 °C where degradation was most active. The values computed for the kinetic parameters, activation energy, E_a, and the pre-exponential factor, A, for each of the runs are shown in Table 4. The reaction models, from Table 2, were applied in the CR method and the model with the highest linearity, R^2, indicated in bold in Table 4, implied that the run closely followed that model. Overall, it can be seen that all of the runs closely followed models in the diffusion category. The non-catalytic run, EFB, with an R^2 of 0.9672, closely followed a one-dimensional diffusion reaction. Yen Yee et al. (2017) previously reported the EFB closely followed the three-dimensional model in their study [34]. The discrepancy between this current study could be due to the amount and particle size of the samples used. The particle sizes of EFB used in this study was 0.5 mm while the particle sizes of EFB used in the study by Yen Yee et al. (2017) was larger. In addition, while Yen Yee et al. (2017) did not report the amount of sample used in the TGA, this study utilized a small amount of EFB, approximately 4 mg, due to instrument limitation, and thus, this could be the reason of obtaining closeness to a one-dimensional diffusion model [34]. For the catalytic runs, all of the runs closely followed the anti-Jander diffusion model with the R^2 order of 0.9712 (EFB-CRHA) > 0.9675 (EFB-NiFeCRHA) > 0.9658 (EFB-FeCRHA) > 0.9644 (EFB-NiCRHA) > 0.9513 (EFB-HZSM-5). An anti-Jander diffusion model is a three-dimensional diffusion reaction where diffusion occurs outward in a spherical particle from inside the particle to the surface layer [35]. This is possible since the catalyst and EFB feedstock were mixed together and the reaction could occur from within the sample mass.

Figure 7 displays the kinetic parameters corresponding to the matter volatilized in Phase II from thermogravimetric analysis for each pyrolysis runs. Following the kinetic parameters obtained based on the highest R^2 for each run, it was seen that overall, the E_a was reduced with the addition of catalysts compared to the non-catalytic run. The non-catalytic run of EFB had an E_a of 74.15 kJ·mol^{-1} which agreed with previous literature utilizing the CR method [36]. Between EFB-HZSM-5 and EFB-CRHA, HZSM-5 catalyst led to a lower E_a (53.81 kJ·mol^{-1}) compared to CRHA (64.28 kJ·mol^{-1}), however, the A value for EFB-CRHA (4.46×10^3 min^{-1}) was higher than that of EFB-HZSM-5 (4.99×10^2 min^{-1}) by two orders of magnitude. For EFB-NiCRHA, although E_a (69.64 kJ·mol^{-1}) was the highest among the catalytic runs,

Table 4 Activation energy and pre-exponential factor for non-catalytic and catalytic EFB pyrolysis

Run	Model	Activation energy (kJ·mol^{-1})	Pre-exponential factor (min^{-1})	R^2
EFB	R0	32.53	8.45×10^1	0.9587
	R1	42.66	1.30×10^3	0.9509
	R2	55.25	3.51×10^4	0.9326
	R3	70.11	1.59×10^6	0.9107
	D1	**74.15**	$\mathbf{4.63 \times 10^5}$	**0.9672**
	D2	78.99	8.16×10^5	0.9660
	D3	87.12	1.42×10^6	0.9626
	D4	82.46	4.32×10^5	0.9647
	D5	67.32	7.45×10^3	0.9585
	D6	102.27	6.51×10^7	0.9533
	PL2	11.72	6.21×10^{-1}	0.9264
	PL3	4.78	6.92×10^{-2}	0.8307
	C1	372.91	1.54×10^3	0.9565
	C2	39.01	1.64×10^2	0.9550
EFB-HZSM-5	R0	26.13	2.01×10^1	0.9281
	R1	37.73	4.92×10^2	0.9070
	R2	52.96	2.74×10^4	0.8754
	R3	71.42	3.14×10^6	0.8450
	D1	61.35	3.37×10^4	0.9450
	D2	67.98	9.43×10^4	0.9397
	D3	76.02	1.67×10^5	0.9317
	D4	70.63	4.18×10^4	0.9371
	D5	**53.81**	$\mathbf{4.99 \times 10^2}$	**0.9513**
	D6	95.12	2.11×10^7	0.9250
	PL2	8.52	2.46×10^{-1}	0.8546
	PL3	2.65	2.55×10^{-2}	0.5776
	C1	31.48	4.49×10^1	0.9197
	C2	33.46	5.16×10^1	0.9159
EFB-CRHA	R0	30.76	5.59×10^1	0.9616
	R1	40.58	8.07×10^2	0.9525
	R2	52.73	1.98×10^4	0.9342
	R3	67.04	7.96×10^5	0.9129
	D1	70.61	2.16×10^5	0.9698
	D2	76.44	4.85×10^5	0.9678
	D3	83.20	6.07×10^5	0.9645
	D4	78.68	1.91×10^5	0.9668
	D5	**64.28**	$\mathbf{4.46 \times 10^3}$	**0.9712**
	D6	97.84	2.50×10^7	0.9549
	PL2	10.83	4.80×10^{-1}	0.9288
	PL3	4.19	5.39×10^{-2}	0.8212
	C1	35.38	9.93×10^1	0.9586
	C2	37.05	1.04×10^2	0.9569
EFB-NiCRHA	R0	33.70	1.14×10^2	0.9528
	R1	45.21	2.45×10^3	0.9357
	R2	60.01	1.14×10^5	0.9055
	R3	77.79	1.03×10^7	0.8732
	D1	76.50	8.04×10^5	0.9619

Table 4 (continued)

Run	Model	Activation energy ($kJ{\cdot}mol^{-1}$)	Pre-exponential factor (min^{-1})	R^2
	D2	83.16	2.20×10^{6}	0.9582
	D3	91.11	3.65×10^{6}	0.9523
	D4	85.79	9.50×10^{5}	0.9564
	D5	**69.64**	$\mathbf{1.48\times10^{4}}$	**0.9644**
	D6	108.65	2.97×10^{8}	0.9363
	PL2	12.30	7.43×10^{-1}	0.9194
	PL3	5.17	8.16×10^{-2}	0.8276
	C1	39.05	2.40×10^{2}	0.9465
	C2	40.48	2.51×10^{2}	0.9431
EFB-FeCRHA	R0	28.13	3.25×10^{1}	0.9525
	R1	39.63	7.54×10^{2}	0.9335
	R2	54.58	3.84×10^{4}	0.9031
	R3	72.62	3.91×10^{6}	0.8725
	D1	65.35	8.08×10^{4}	0.9631
	D2	71.96	2.24×10^{5}	0.9588
	D3	79.93	3.84×10^{5}	0.9522
	D4	74.60	9.81×10^{4}	0.9568
	D5	**58.77**	$\mathbf{1.53\times10^{3}}$	**0.9658**
	D6	97.57	3.37×10^{7}	0.9352
	PL2	9.52	3.36×10^{-1}	0.9076
	PL3	3.31	3.66×10^{-2}	0.7412
	C1	33.46	7.10×10^{1}	0.9452
	C2	35.42	8.07×10^{1}	0.9417
EFB-NiFeCRHA	R0	30.67	5.97×10^{1}	0.9559
	R1	42.80	1.58×10^{3}	0.9381
	R2	58.71	9.94×10^{4}	0.9062
	R3	77.96	1.33×10^{7}	0.8734
	D1	70.43	2.47×10^{5}	0.9652
	D2	77.37	7.36×10^{5}	0.9615
	D3	85.78	1.39×10^{6}	0.9552
	D4	80.15	3.32×10^{5}	0.9596
	D5	**63.57**	$\mathbf{4.44\times10^{3}}$	**0.9675**
	D6	104.47	1.54×10^{8}	0.9382
	PL2	10.79	4.95×10^{-1}	0.9194
	PL3	4.16	5.47×10^{-2}	0.8019
	C1	36.27	1.38×10^{2}	0.9495
	C2	38.34	1.60×10^{2}	0.9462

Rows indicated in bold highlight the model with the highest linearity and its resulting activation energy and pre-exponential factor for each run

the A value (1.48×10^{4} min^{-1}) was also the highest among the catalytic runs, and consequently resulted in the highest amount of volatilized matter in Phase II (71.5 wt%) as seen in Fig. 7. Since the A value represents the rate of collision of particles, namely the volatilized matter, during the reaction, the higher A value determined for EFB-NiCRHA could indicate that the collision of particles was rapid to the point

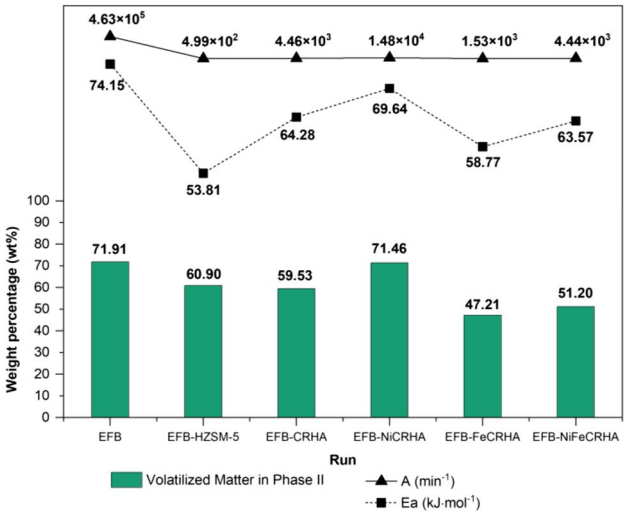

Fig. 7 Comparison of activation energies and pre-exponential factors with the corresponding amount of volatilized matter in Phase II obtained from thermogravimetric analysis for non-catalytic and catalytic EFB pyrolysis runs over HZSM-5 and synthesized catalysts

that the energy barrier was able to be overcome despite the relatively high value of E_a [37]. EFB-FeCRHA, on the other hand, compared to the catalytic run over metal-modified catalysts, had the lowest E_a (58.77 $kJ{\cdot}mol^{-1}$) and A value (1.53×10^{3} min^{-1}), which resulted in very low total volatilized matter in Phase II, as seen in Fig. 7. For EFB-NiFeCRHA, E_a and the A value obtained was between that of the runs with metal-modified catalysts and thus, the volatilized matter in Phase II achieved was also between that of the runs with metal-modified catalysts.

Based on the synthesized catalysts that have been tested in this study, it can be seen that CRHA has similar features to HZSM-5 and behaves similarly to it. When CRHA is metal-modified, NiCRHA appeared to be the best in catalytic cracking and had the highest rate of particle collision despite higher E_a among the catalytic runs, resulting in more volatilized matter in Phase II than FeCRHA and NiFeCRHA. On the other hand, FeCRHA was the least effective catalyst in cracking the pyrolysis vapours due to lowest amount volatilized matter achieved in Phase II.

4 Conclusions

Rice husk ash (RHA) was successfully applied as a silica source for the synthesis of catalyst CRHA. From the characterization results, CRHA was similar in structure to the HZSM-5 catalyst. CRHA was metal modified with both nickel and iron species and individually. Characterization results showed that the parent catalyst structure was not affected but the surface area and porosity properties were reduced.

The synthesized catalysts were applied to the pyrolysis of empty fruit bunch (EFB). Using a thermogravimetric analyser, CRHA behaved similarly to HZSM-5 catalyst in degrading EFB, where CRHA produced 75.1 wt% total volatilized matter while HZSM-5 produced 73.3 wt% total volatilized matter. Between the metal-modified catalysts, NiCRHA produced the highest amount of total volatilized matter of 83.9 wt%, due to the higher cracking ability of nickel species while FeCRHA achieved the lowest amount of total volatilized matter of 56.1 wt%.

From the application of various kinetic models using Coats-Redfern method, the pyrolysis runs generally followed the diffusion model, where the non-catalytic run followed a one-dimensional diffusion and the catalytic runs followed a three-dimensional anti-Jander diffusion model. From kinetic analysis, the addition of catalysts generally showed reduction of activation energy compared to the non-catalytic run (74.15 $kJ{\cdot}mol^{-1}$) ranging between 53.81 $kJ{\cdot}mol^{-1}$ to 69.64 $kJ{\cdot}mol^{-1}$. Although the catalytic run using NiCRHA had the highest activation energy (69.64 $kJ{\cdot}mol^{-1}$), the highest pre-exponential factor computed (1.48×10^4 min^{-1}) when NiCRHA was used allowed the reaction to overcome the energy barrier and produced the most volatilized matter in Phase II. Due to the different cracking abilities of the metal-modified catalysts, further analysis on the volatilized matter should be conducted to observe how the different catalysts affect the chemical composition of the volatilized matter.

Overall, this study showed that not only catalysts can be synthesized using natural, renewable resources, it can also be applied to pyrolysis processes, where the synthesized catalysts behave similarly to conventional catalyst. In addition, the metal-modification, especially using nickel, on the parent catalyst CRHA had improved the cracking ability of the catalyst in the pyrolysis process and showed the highest cracking ability when compared to the other metal-modification, using iron and bi-metallic nickel–iron. Thus, the findings from this study can be applied to future studies exploring the catalyst performance in biomass pyrolysis products. Finally, agricultural by-products that are otherwise discarded have shown to be useful in catalyst synthesis.

Acknowledgements The authors would like to thank Universiti Teknologi Malaysia (UTM) for the financial support to carry out this research project.

Authors' contributions Nadhilah Aqilah Shahdan contributed to the conducting of the experiments and writing. Vekes Balasundram contributed to the supervision of the experiments, data analysis and editing of this manuscript. Norazana Ibrahim contributed to the data analysis and writing. Ruzinah Isha contributed to the writing and editing of the manuscript.

Funding Funding for this research was received from Universiti Teknologi Malaysia under the Research University Grant—UTM ER (Vot number: Q.K130000.3843.19J46).

Data availability This declaration is not applicable for this study.

Declarations

Ethical approval This declaration is not applicable for this study.

Competing interests The authors declare no competing interests.

References

1. Bian R, Ma B, Zhu X, Wang W, Li L, Joseph S, Liu X, Pan G (2016) Pyrolysis of crop residues in a mobile bench-scale pyrolyser: Product characterization and environmental performance. J Anal Appl Pyrolysis 119:52–59. https://doi.org/10.1016/j.jaap.2016.03.018
2. Hassan H, Hameed BH, Lim JK (2020) Co-pyrolysis of sugarcane bagasse and waste high-density polyethylene: Synergistic effect and product distributions. Energy 191:116545. https://doi.org/10.1016/j.energy.2019.116545
3. Ro D, Kim Y-M, Lee I-G, Jae J, Jung S-C, Kim SC, Park Y-K (2018) Bench scale catalytic fast pyrolysis of empty fruit bunches over low cost catalysts and HZSM-5 using a fixed bed reactor. J Clean Prod 176:298–303. https://doi.org/10.1016/j.jclepro.2017.12.075
4. Ozturk M, Saba N, Altay V, Iqbal R, Hakeem KR, Jawaid M, Ibrahim FH (2017) Biomass and bioenergy: An overview of the development potential in Turkey and Malaysia. Renew Sustain Energy Rev 79:1285–1302. https://doi.org/10.1016/j.rser.2017.05.111
5. Hamzah N, Tokimatsu K, Yoshikawa K (2019) Solid Fuel from Oil Palm Biomass Residues and Municipal Solid Waste by Hydrothermal Treatment for Electrical Power Generation in Malaysia: A Review. Sustainability 11(4). https://doi.org/10.3390/su11041060
6. James Rubinsin N, Daud WRW, Kamarudin SK, Masdar MS, Rosli MI, Samsatli S, Tapia JF, Wan AB, Karim Ghani WA, Lim KL (2020) Optimization of oil palm empty fruit bunches value chain in Peninsular Malaysia. Food Bioprod Process 119:179–194. https://doi.org/10.1016/j.fbp.2019.11.006
7. Bhoi PR, Ouedraogo AS, Soloiu V, Quirino R (2020) Recent advances on catalysts for improving hydrocarbon compounds in bio-oil of biomass catalytic pyrolysis. Renew Sustain Energy Rev 121:109676. https://doi.org/10.1016/j.rser.2019.109676
8. Chang SH (2018) Bio-oil derived from palm empty fruit bunches: Fast pyrolysis, liquefaction and future prospects. Biomass Bioenerg 119:263–276. https://doi.org/10.1016/j.biombioe.2018.09.033
9. Uzoejinwa BB, He X, Wang S, El-Fatah Abomohra A, Hu Y, Wang Q (2018) Co-pyrolysis of biomass and waste plastics as a thermochemical conversion technology for high-grade biofuel production: Recent progress and future directions elsewhere worldwide. Energy Convers Manag 163:468–492. https://doi.org/10.1016/j.enconman.2018.02.004
10. Kan T, Strezov V, Evans T, He J, Kumar R, Lu Q (2020) Catalytic pyrolysis of lignocellulosic biomass: A review of variations in process factors and system structure. Renew Sustain Energy Rev 134:110305. https://doi.org/10.1016/j.rser.2020.110305
11. Persson H, Duman I, Wang S, Pettersson LJ, Yang W (2019) Catalytic pyrolysis over transition metal-modified zeolites: A comparative study between catalyst activity and deactivation. J Anal Appl Pyrolysis 138:54–61. https://doi.org/10.1016/j.jaap.2018.12.005
12. Li Y, Nishu, Yellezuome D, Li C, Liu R (2022) Deactivation mechanism and regeneration effect of bi-metallic Fe-Ni/ZSM-5 catalyst during biomass catalytic pyrolysis. Fuel 312:122924. https://doi.org/10.1016/j.fuel.2021.122924

13. Sriatun, Susanto H, Widayat, Darmawan A (2019) Characteristic of ZSM-5 catalyst supported by nickel and molybdenum. IOP Conf. Series: Mater. Sci. Eng. 509(1):012138. https://doi.org/10.1088/1757-899X/509/1/012138
14. Li X, Dong W, Zhang J, Shao S, Cai Y (2020) Preparation of bio-oil derived from catalytic upgrading of biomass vacuum pyrolysis vapor over metal-loaded HZSM-5 zeolites. J Energy Inst 93(2):605–613. https://doi.org/10.1016/j.joei.2019.06.005
15. Widayat W, Annisa AN (2017) Synthesis and Characterization of ZSM-5 Catalyst at Different Temperatures. IOP Conf. Series: Mater. Sci. Eng. 214:012032. https://doi.org/10.1088/1757-899x/214/1/012032
16. Korotkova TG, Ksandopulo SJ, Donenko AP, Bushumov SA, Danilchenko AS (2016) Physical Properties and Chemical Composition of the Rice Husk and Dust. Orient J Chem 32(6):3213–3219
17. Dey KP, Ghosh S, Naskar MK (2013) Organic template-free synthesis of ZSM-5 zeolite particles using rice husk ash as silica source. Ceram Int 39(2):2153–2157. https://doi.org/10.1016/j.ceramint.2012.07.083
18. Zhang C, Li S, Bao S (2019) Sustainable Synthesis of ZSM-5 Zeolite from Rice Husk Ash Without Addition of Solvents. Waste Biomass Valorization 10(10):2825–2835. https://doi.org/10.1007/s12649-018-0356-0
19. Saadatkhah N, Carillo Garcia A, Ackermann S, Leclerc P, Latifi M, Samih S, Patience GS, Chaouki J (2020) Experimental methods in chemical engineering: Thermogravimetric analysis—TGA. The Canadian Journal of Chemical Engineering 98(1):34–43. https://doi.org/10.1002/cjce.23673
20. Vyazovkin S, Burnham AK, Criado JM, Pérez-Maqueda LA, Popescu C, Sbirrazzuoli N (2011) ICTAC Kinetics Committee recommendations for performing kinetic computations on thermal analysis data. Thermochim Acta 520(1):1–19. https://doi.org/10.1016/j.tca.2011.03.034
21. Raza M, Abu-Jdayil B, Al-Marzouqi AH, Inayat A (2022) Kinetic and thermodynamic analyses of date palm surface fibers pyrolysis using Coats-Redfern method. Renew Energy 183:67–77. https://doi.org/10.1016/j.renene.2021.10.065
22. Shahdan NA, Balasundram V, Ibrahim N, Isha R, Manan ZA (2022) Catalytic Co-pyrolysis of empty fruit bunch and high-density polyethylene mixtures over rice husk ash: Thermogravimetric, kinetic and thermodynamic analyses. Cleaner Engineering and Technology 9:100538. https://doi.org/10.1016/j.clet.2022.100538
23. Li Y, Nishu YD, Chai M, Li C, Liu R (2021) Catalytic pyrolysis of biomass over Fe-modified hierarchical ZSM-5: Insights into mono-aromatics selectivity and pyrolysis behavior using Py-GC/MS and TG-FTIR. J Energy Inst 99:218–228. https://doi.org/10.1016/j.joei.2021.09.013
24. Vichaphund S, Aht-ong D, Sricharoenchaikul V, Atong D (2014) Catalytic upgrading pyrolysis vapors of Jatropha waste using metal promoted ZSM-5 catalysts: An analytical PY-GC/MS. Renew Energy 65:70–77. https://doi.org/10.1016/j.renene.2013.07.016
25. Balasundram V, Ibrahim N, Kasmani RM, Hamid MKA, Isha R, Hasbullah H, Ali RR (2017) Thermogravimetric catalytic pyrolysis and kinetic studies of coconut copra and rice husk for possible maximum production of pyrolysis oil. J Clean Prod 167:218–228. https://doi.org/10.1016/j.jclepro.2017.08.173
26. Cheng S, Wei L, Julson J, Muthukumarappan K, Kharel PR (2017) Upgrading pyrolysis bio-oil to hydrocarbon enriched biofuel over bifunctional Fe-Ni/HZSM-5 catalyst in supercritical methanol. Fuel Process Technol 167:117–126. https://doi.org/10.1016/j.fuproc.2017.06.032
27. Balasundram V, Zaman KK, Ibrahim N, Kasmani RM, Isha R, Hamid MKA, Hasbullah H (2018) Catalytic upgrading of pyrolysis vapours over metal modified HZSM-5 via in-situ pyrolysis of sugarcane bagasse: Effect of nickel to cerium ratio on HZSM-5. J Anal Appl Pyrolysis 134:309–325. https://doi.org/10.1016/j.jaap.2018.06.021
28. Chen B-H, Chao Z-S, He H, Huang C, Liu Y-J, Yi W-J, Wei X-L, An J-F (2016) Towards a full understanding of the nature of Ni(ii) species and hydroxyl groups over highly siliceous HZSM-5 zeolite supported nickel catalysts prepared by a deposition–precipitation method. Dalton Trans 45(6):2720–2739. https://doi.org/10.1039/C4DT00399C
29. Nishu LY, Liu R (2022) Catalytic pyrolysis of lignin over ZSM-5, alkali, and metal modified ZSM-5 at different temperatures to produce hydrocarbons. J Energy Inst 101:111–121. https://doi.org/10.1016/j.joei.2022.01.001
30. Brunauer S, Emmett PH, Teller E (1938) Adsorption of Gases in Multimolecular Layers. J Am Chem Soc 60(2):309–319. https://doi.org/10.1021/ja01269a023
31. Barrett EP, Joyner LG, Halenda PP (1951) The Determination of Pore Volume and Area Distributions in Porous Substances I Computations from Nitrogen Isotherms. J Am Chem Soc 73(1):373–380
32. Wang Z, Burra KG, Lei T, Gupta AK (2021) Co-pyrolysis of waste plastic and solid biomass for synergistic production of biofuels and chemicals-A review. Prog Energy Combust Sci 84:100899. https://doi.org/10.1016/j.pecs.2020.100899
33. Hamzah NS, Idris SS, Rahman NA, Abu Bakar NF, Matali S (2021) Thermal Analysis of Co-Utilization of Empty Fruit Bunch and Silantek Coal Under Inert Atmosphere Using Thermogravimetric Analyzer (TGA). Frontiers in Energy Research 8. https://doi.org/10.3389/fenrg.2020.608756
34. Yen Yee C, Suchithra T-G, Suyin G, Hoon Kiat N, Lai Yee L (2017) Synergic Effect and Kinetic Mechanisms for Co-Pyrolysis of Empty Fruit Bunch and Palm Oil Sludge. The Journal of The Institution of Engineers, Malaysia 78(1). https://doi.org/10.54552/v78i1.11
35. Dickinson CF, Heal GR (1999) Solid–liquid diffusion controlled rate equations. Thermochim Acta 340–341:89–103. https://doi.org/10.1016/S0040-6031(99)00256-7
36. Yiin CL, Yusup S, Quitain AT, Uemura Y, Sasaki M, Kida T (2018) Thermogravimetric analysis and kinetic modeling of low-transition-temperature mixtures pretreated oil palm empty fruit bunch for possible maximum yield of pyrolysis oil. Bioresour Technol 255:189–197. https://doi.org/10.1016/j.biortech.2018.01.132
37. Zhang S, Liang Y, Qian X, Hui D, Sheng K (2020) Pyrolysis kinetics and mechanical properties of poly(lactic acid)/bamboo particle biocomposites: Effect of particle size distribution. Nanotechnol Rev 9(1):524–533. https://doi.org/10.1515/ntrev-2020-0037